European Journal of Prosthodontics and Restorative Dentistry (2026) 34 (5s), 27–42

Anethum graveolens-Mediated Biosynthesis of Zinc Oxide Nanoparticles Incorporated in Bone Shell Scaffolds: In Vitro Evaluation of Osteogenic and Antimicrobial Properties

Keywords
Antibacterial activity, Bone shell scaffold, Bone regeneration, Green synthesis, Osteogenic differentiation, Zinc oxide nanoparticles.

Luay A. Hussein[1*]
B.D.S, MSc, PhD Candidate of Oral Surgery, Oral and Maxillofacial Department, College of Dentistry, Hawler Medical University, Erbil, Kurdistan Region, Iraq
Email: luay.hussein@den.hmu.edu.krd

Othman A. Omar[2]
B.D.S, FIBMS, Oral and Maxillofacial Department, College of Dentistry, Hawler Medical University, Erbil, Kurdistan Region, Iraq

Azeez A. Barzinjy[3]
Department of Physics, Faculty of Science, Soran University, Kurdistan region, Iraq/ Department of Physics Education, Faculty of Education, Tishk International University, Erbil, Iraq

*Corresponding author:

Luay Ahmed Hussein

B.D.S, MSc, PhD candidate of oral surgery, Oral and Maxillofacial Department, Hawler Medical University, College of Dentistry, Erbil, Kurdistan Region, Iraq
Email: luay.hussein@den.hmu.edu.krd

Received: 06-04-2026
Revised: 18-05-2026
Accepted:13-06-2026
Doi: 10.1922/ejprd.v34i5s.1535

ABSTRACT

Objectives: To synthesize zinc oxide nanoparticles (ZnO NPs) using Anethum graveolens extract via a green approach, coat them onto cortical bone shell scaffolds, and evaluate their physicochemical properties, cytocompatibility, osteogenic potential, and antimicrobial activity compared with commercial ZnO NPs.

Methods: Green ZnO NPs were synthesized using A. graveolens extract and characterized by SEM, TEM, XRD, FTIR, UV–Vis, BET, EDS, and zeta potential analyses. Nanoparticles were coated onto cortical bone plates. Antibacterial and antibiofilm activities against Streptococcus mutans and Staphylococcus aureus were assessed. Cytocompatibility was evaluated using an MTT assay in MG-63 cells. Osteogenic activity was examined by real-time PCR analysis of ALP, COL1, and OCN expression and by Alizarin Red S staining.

Results: Green ZnO NPs exhibited nanoscale size, porous morphology, mesoporous structure, and improved colloidal stability. Coating of cortical bone scaffolds was successfully confirmed. Compared with commercial ZnO NPs, green ZnO NPs showed lower cytotoxicity, enhanced expression of osteogenic markers, greater matrix mineralization, and stronger antibacterial and antibiofilm effects, particularly against S. aureus.

Conclusions: Green-synthesized ZnO NPs demonstrated favorable physicochemical characteristics, superior biocompatibility, enhanced osteogenic performance, and improved antimicrobial activity, supporting their potential as bioactive coatings for bone tissue engineering applications.

1. INTRODUCTION

Bone defects from trauma, tumors, infection, or birth defects make reconstructive surgery difficult. Bone can regrow, but large defects require surgery. Autografts, the standard treatment, are limited by donor site, availability, immune rejection, and disease risk (1,2). These limitations have encouraged the development of advanced biomaterials that mimic the natural bone microenvironment and promote faster healing. In this context, nanotechnology has emerged as an important approach in tissue engineering, since nanoparticles with sizes of 1–100 nm possesses unique physicochemical properties, including a high surface-to-volume ratio, increased reactivity, and enhanced interactions with cells, all of which can improve tissue regeneration (3). Nano material-based scaffolds improve osteoblast adhesion, proliferation, and differentiation, improving bone regeneration (4). Zinc oxide nanoparticles (ZnO NPs) are popular due to their biocompatibility, stability, and multifunctionality.

Zinc is an essential trace element that cofactors over 300 enzymes that regulate DNA synthesis, protein production, and cell cycle progression (5). In bone metabolism, zinc promotes osteoblast proliferation, collagen synthesis, alkaline phosphatase activity, and matrix mineralization (6). ZnO nanoparticles release Zn^{2+} ions that activate osteogenic pathways, promote angiogenesis, and support mineral deposition, aiding bone regeneration (7). However, conventional chemical synthesis of ZnO nanoparticles uses hazardous chemicals and energy-intensive processes, raising environmental and safety concerns. Green synthesis offers an eco-friendly alternative by using plant-derived phytochemicals as natural reducing and stabilizing agents, improving biocompatibility and biological functionality (8,9). Anethum graveolens (dill), rich in antioxidant and antimicrobial phytochemicals, is a promising candidate for green ZnO nanoparticle synthesis. These natural compounds enhance nanoparticle stability and bioactivity. Meanwhile, bone tissue engineering favors bone-derived scaffolds that mimic native bone and require high biocompatibility, interconnected porosity, suitable strength, osteoconductivity, and controlled biodegradability (10). Incorporation of bioactive nanoparticles such as ZnO may further enhance osteogenesis while providing antibacterial properties and improving scaffold performance (11). The use of green-synthesized ZnO nanoparticles in bone scaffolds lacks comprehensive evaluation. Therefore, this study synthesized ZnO nanoparticles via an Anethum graveolens green approach to coat bone shell matrices. We compared the osteogenic and antibacterial properties of these plant-derived nanoparticles against commercial ZnO to highlight the potential of green nanotechnology in bone regeneration.

2. EXPERIMENTAL APPROACH

2.1. Materials

SDS (Sigma-Aldrich, USA) was used as a stabilizer and zinc acetate dihydrate ($Zn(CH_3COO)_2 \cdot 2H_2O$; Merck, Germany) as the zinc precursor. Reference was US Research Nanomaterials' commercial ZnO nanoparticles. The preparation used absolute ethanol (Merck, Germany) and phosphate-buffered saline (PBS; pH 7.2–7.4; Sigma-Aldrich, USA). Cortical plate allograft bone plates (1.2 × 1 cm; CenoBone, KFZ) served as substrates. All steps utilized deionized water (≥18 MΩ·cm). Anethum graveolens leaf extract was used fresh or stored at 4 °C in the dark as a green capping agent.

2.2. Characterization Techniques

XRD analysis was performed with a PANalytical X'Pert PRO (Cu Kα, 1.5406 Å; 2θ: 20°–80°, 1°/min). SEM (FEI Quanta 450) assessed particle distribution. Elemental composition was determined by EDX (Bruker XFlash® 6-10, QUANTAX). FTIR spectra were recorded on a Shimadzu ATR-FTIR (single-bounce diamond ATR, 4 cm^{-1} resolution). UV–Vis spectra were collected with a Cecil Aquarius CE 9500 (190–1100 nm, 1 cm quartz cuvettes, baseline corrected). TEM (Zeiss EM10, 100 kV). Nitrogen adsorption–desorption (BELSORP-mini II, 77 K) with AFSM™ correction evaluated textural properties. Zeta potential was measured at room temperature using a HORIBA SZ-100 nanoparticle analyzer.

2.3. Methods

2.3.1. Synthesis of green ZnO Nanostructures

To synthesize green ZnO nanostructures, 20 g of Anethum graveolens was Soxhlet-extracted with 200 mL distilled water for 5 h. Then, 1.0 g zinc acetate dihydrate in 50 mL double-distilled water was mixed with 25 mL plant extract, stirred for 10 min, followed by addition of 0.1 g SDS. The mixture was heated at 60 °C for 60 min, and the obtained precipitate was calcined at 400 °C for 2 h. After cooling, it was dispersed in 25 mL ethanol, sonicated for 10 min, centrifuged at 9,000 rpm for 5 min, and dried at 85 °C for 1 h (scheme1).

2.3.2. Surface Coating of Cortical Plate Allograft

PBS (pH 7.2–7.4) was used to prepare and coat cortical plate allograft samples (1.2 × 1 cm). The samples were cleaned by sonication in ethanol and PBS for 5 min each and then air-dried. Next, 0.010 g of commercial or green ZnO nanoparticles was dispersed in 100 mL sterile PBS (100 µg/mL stock), filtered, and diluted. Bone plates were immersed in the suspension, vacuum-treated for 3 min, sonicated under vacuum for 3 min, then sonicated again for 5 min and left for 5 h for ZnO deposition. The coated plates were finally dried at room temperature (scheme2).

2.4. In vitro antibacterial activity test

The antibacterial activity of green-synthesized and commercial zinc oxide nanoparticles (ZnO NPs) was evaluated against Streptococcus mutans (ATCC 12725) and Staphylococcus aureus (ATCC 25923). Bacterial suspensions were standardized to 0.5 McFarland (≈1.5 × 10^8 CFU/mL) prior to testing.

2.4.1. Minimum Inhibitory Concentration (MIC)

MIC values were determined using the broth microdilution method in sterile 96-well plates. Nanoparticle stock solutions (2 mg/mL) were serially diluted to concentrations ranging from 10–100 µg/mL. Each well contained Mueller–Hinton broth and bacterial suspension and was incubated at 37 °C for 24 h. Bacterial growth inhibition was assessed by measuring optical density at 600 nm, and the MIC was defined as the lowest concentration preventing visible growth.

2.4.2. Agar Well Diffusion Assay

Antibacterial activity was further evaluated using the agar well diffusion method. Mueller–Hinton agar plates were inoculated with bacterial suspensions, and 6-mm wells were filled with 100 µL of nanoparticle solutions at different concentrations (10–100 µg/mL). Chlorhexidine (0.2%) served as the positive control. Plates were incubated at 37 °C for 24 h, and inhibition zones were measured in millimeters.

2.4.3. Antibiofilm Assay

Antibiofilm activity was determined using a microtiter plate crystal violet assay. Bacterial suspensions (~10^6 CFU/mL) were incubated with ZnO nanoparticles at different concentrations for 24 h at 37 °C. Biofilms were stained with 0.1% crystal violet, and absorbance was

measured at 600 nm to determine the percentage inhibition of biofilm formation.

2.5. Cell Viability/ Cell toxicity analysis

MG-63 cells (1×10^4/well) were incubated for 16 h, then treated with varying doses of commercial ZnO, green ZnO, or cisplatin (control) for 72 h. Cell viability was assessed in triplicate by adding MTT for 4 h, dissolving the resulting crystals in DMSO, and measuring absorbance at 570 and 630 nm.

2.5.1. Real-Time PCR

Gene expression of ALP, COL1, and osteocalcin in MG-63 cells treated with commercial and green ZnO NPs was analyzed by real-time PCR. MG-63 cells (5×10^5 cells/well) were seeded in 6-well plates, treated with varying concentrations of ZnO NPs (commercial: 0, 5, 10 µg/mL; green: 0, 50, 100 µg/mL), and incubated for 1, 3, and 7 days. Total RNA was extracted using RNAzol, assessed for purity/concentration (A260/280), and stored at −70 °C. cDNA was synthesized from 1 µg RNA, and quantitative PCR was performed with SYBR Green Master Mix. GAPDH served as the internal control.

Relative changes in target gene expression were calculated using the ΔΔCt method. The primer sequences are listed in (Table 1).

2.5.2. Alizarin Red S staining

Mineralization in MG-63 cells was assessed by Alizarin Red S staining. Cells (5×10^4/well) were seeded in 6-well plates, incubated 24 h, then treated with commercial (0, 10 µg/mL) or green ZnO NPs (0, 100 µg/mL) for 1, 3, or 7 days. After treatment, cells were washed with PBS, fixed in 70% ethanol (20 min), stained with ARS (40 mM, pH 4.2, 10 min), rinsed, and examined by light microscopy.

3. RESULTS

3.1. Morphology and Structural Characterization

3.1.1. SEM morphology analysis

SEM revealed that green ZnO had a rough, porous, cauliflower-like structure with loosely packed agglomerates, while commercial ZnO was more compact and heterogeneous, with a smaller particle size of ~38 nm versus ~61 nm for green ZnO (Fig.1). On bone plates, green ZnO formed a more continuous and uniform porous coating, whereas commercial ZnO showed discontinuous deposition with localized agglomeration (Fig.2). Uncoated bone plates displayed a dense lamellar morphology without nanoparticles.

3.2. TEM analysis

3.2.1. TEM analysis of green-synthesized ZnO nanoparticles

TEM analysis showed that green-synthesized ZnO nanoparticles were mostly quasi-spherical to slightly irregular and formed chain-like aggregates at low magnification. The primary particles were relatively uniform, with a unimodal size distribution and a mean size of ~21 nm (20.56 ± 7.32 nm) (Fig.3). These TEM sizes were smaller than the agglomerate sizes seen by SEM, indicating that the material consisted of nanosized primary particles assembled into clusters.

3.2.2. TEM analysis of commercial ZnO nanoparticles

TEM images of commercial ZnO nanoparticles revealed quasi-spherical, chain-like agglomerates composed of uniform primary particles (~18 nm, 17.82 ± 6.90 nm) (Fig.4). Aggregation was due to ZnO's high surface energy and sample prep. Particle sizes were smaller than SEM values, and were slightly smaller but morphologically similar to green-synthesized ZnO.

3.3. BET surface area and pore structure analysis

Both commercial and green-synthesized ZnO showed type IV nitrogen adsorption–desorption isotherms with hysteresis, confirming mesoporosity (Fig.5). Commercial ZnO had a higher surface area of 17.43 m^2/g than green ZnO (12.16 m^2/g), while both had similar pore volumes of ~0.14 cm^3/g. Green ZnO showed a larger mean pore diameter of 45.74 nm compared with 32.22 nm for commercial ZnO. Both samples had negligible microporosity, indicating mainly interparticle mesopores.

3.4. FTIR analysis

FTIR spectra of uncoated bone plates showed typical collagen and apatite bands (Fig.6). Commercial ZnO displayed mainly Zn–O stretching, indicating a mostly inorganic composition. Green-synthesized ZnO showed additional O–H/N–H, carbonyl/amide, and carbonate/carboxylate bands, reflecting phytochemical capping agents. Coated bone plates exhibited combined bone and ZnO features, confirming effective ZnO coating while preserving the bone matrix. Reduced intensity of some organic bands suggests partial surface coverage by ZnO.

3.5. XRD analysis of uncoated and ZnO-coated bone plates

XRD analysis showed that the uncoated bone plate had a broad amorphous pattern without distinct Bragg peaks (Fig.7). The commercial ZnO-coated bone plate displayed weak ZnO peaks at $2\theta = 31.1807°$ and 35.7546° with d-spacings of 2.8685 Å and 2.5114 Å, confirming crystalline zincite ZnO (98-006-5122). The green-ZnO-coated bone plate exhibited more intense and numerous peaks at $2\theta = 31.0218°$, 33.7225°, 35.6355°, 46.6818°, 55.9154°, and 62.1359°, consistent with the wurtzite ZnO phase (98-003-1060)15. The increased number and clarity of peaks indicate improved crystallinity, higher surface loading, and/or more uniform coating compared with the commercial ZnO.

The stronger ZnO reflections observed in the green-coated sample indicate better coating efficiency, which is consistent with the SEM results.

Crystallite size was estimated using the Scherrer equation (1) with $K = 0.94$ and $\lambda = 0.15406$ nm. The average crystallite size was ~10.10 nm for commercial ZnO and ~16.17 nm for green ZnO, (Table 2), (Table 3).

3.6. UV–Vis absorption and optical band gap analysis

UV–Vis spectra showed strong UV absorption for both ZnO samples, typical of ZnO nanoparticles. Commercial ZnO had an absorption maximum at ~373 nm, while green-synthesized ZnO showed a red-shifted maximum at ~378 nm. The estimated optical band gaps were 2.93 eV for commercial ZnO and 2.64 eV for green ZnO (Fig.8). The lower band gap and red shift in green ZnO are likely

due to defect states, surface disorder, and phytochemical residues from green synthesis. These features suggest increased surface-related states and may enhance visible-light absorption. TEM and UV–Vis results both indicate that commercial ZnO has a slightly smaller particle size and higher band gap compared to green ZnO.

3.7. EDX elemental analysis of uncoated and ZnO-coated bone plates

EDX analysis of uncoated bone plates showed strong Ca, P, and O peaks, consistent with cortical bone. After ZnO coating, Zn peaks appeared in both commercial and green-ZnO samples, confirming successful deposition (Fig.9). The green-ZnO-coated sample showed more intense Zn signals, indicating higher loading or better coverage. Elemental mapping revealed a uniform Zn distribution along with Ca, P, and O from the bone, confirming homogeneous coating. Ag signals were attributed to sample prep.

3.8. Zeta potential analysis of ZnO nanoparticles

Both commercial and green-synthesized ZnO nanoparticles showed negative zeta potentials, indicating negatively charged surfaces. Commercial ZnO had −19.1 mV, while green ZnO was slightly more negative at −21.3 mV, suggesting marginally better colloidal stability (Fig.10). Both values indicate moderate stability with some aggregation possible. Overall, green ZnO showed a slight advantage in dispersion stability.

3.9. Cytotoxicity effect of green and commercial ZnONPs on human osteoblast-like MG-63 Cells

Green-synthesized ZnO showed high cytocompatibility with MG-63 cells, maintaining >90% viability up to 125 µg/mL and an IC_{50} of 321.9 ± 22.8 µg/mL (Fig.11). Commercial ZnO was more toxic (IC_{50} = 26.11 ± 2.21 µg/mL), while cisplatin was the most cytotoxic (IC_{50} = 7.16 ± 0.86 µg/mL). The much higher IC_{50} of green ZnO suggests superior biocompatibility, likely due to phytochemical surface capping, making it more suitable for bone plate coatings than commercial ZnO.

3.10. The osteogenic effects of green and commercial ZnONPs on human osteoblast-like MG-63 cells

Green-synthesized ZnO showed enhanced osteogenic potential, with higher ALP, COL1, and OCN expression at 1, 3, and 7 days compared to commercial ZnO. This is likely due to improved surface chemistry, controlled Zn^{2+} release, and reduced oxidative stress. Green ZnO combines better cytocompatibility, antibacterial activity, and osteogenic effects, supporting its use in bone tissue engineering and antimicrobial coatings.

3.10.1 ALP Activity (Early Osteogenic Marker)

Fig. 12 shows that ALP expression increased in a time- and dose-dependent manner in both groups, with significantly greater upregulation in green ZnO-treated cells. Green ZnO (50 and 100 µg/mL) produced markedly higher fold increases than commercial ZnO (5 and 10 µg/mL), particularly at Day 7 (****), indicating enhanced early osteoblastic differentiation and matrix maturation. In contrast, commercial ZnO induced only modest ALP expression, reflecting lower osteoinductive potential.

3.10.2 COL1 Expression (Matrix Formation Marker)

Fig.13 showed COL1 expression progressively increased from Day 1 to Day 7 in all treated groups. Green ZnO nanoparticles promoted significantly greater collagen synthesis and extracellular matrix production than commercial ZnO across all time points. This highlights the superior capacity of green ZnO to support critical bone tissue formation.

3.10.3 OCN Expression (Late Osteogenic Marker)

Green ZnO NPs significantly enhanced late-stage osteogenic differentiation (OCN expression) compared to commercial ZnO, which demonstrated reduced efficiency and higher cytotoxicity (Fig.14).

3.10.4 Osteogenic Differentiation of MG-63 Cells in Response to Green and Commercial ZnO

Green ZnO NPs (50–100 µg/mL) significantly upregulated ALP and COL1 expression compared to commercial ZnO, indicating enhanced extracellular matrix formation. Furthermore, green ZnO sustained OCN expression over time, whereas commercial ZnO showed reduced expression at later stages. These findings confirm that green ZnO promotes stronger osteogenic differentiation and matrix maturation.

This effect is likely related to the biological role of Zn^{2+} ions in stimulating osteoblast activity and matrix mineralization, together with phytochemical surface functionalization that regulates ion release and improves biocompatibility. Controlled Zn^{2+} release has also been associated with activation of osteogenic signaling pathways. Overall, green-synthesized ZnO provides a favorable microenvironment for osteogenesis, supporting its potential in bone tissue engineering and biomaterial coatings.

3.11. Extracellular Matrix Mineralization in MG-63 Cells Treated with Green and Commercial ZnO Nanoparticles

Fig. 15 showed the extent of extracellular matrix mineralization in MG-63 cells treated with green synthesized and commercial ZnO nanoparticles was evaluated using Alizarin Red S (ARS) staining at Days 1, 3, and 7. ARS specifically binds to calcium deposits, thereby serving as an indicator of late-stage osteogenic differentiation and matrix mineralization.

3.11.1 Green ZnO Nanoparticle-Treated Group

In the green ZnO-treated group (Fig. 15), minimal mineral deposition was observed at Day 1, with a moderate increase by Day 3. By Day 7, intense and uniformly distributed ARS staining indicated substantial calcium nodule formation. These findings demonstrate that green-synthesized ZnO significantly enhances mineralization and osteogenic maturation over time.

3.11.2 Commercial ZnO Nanoparticle-Treated Group

MG-63 cells treated with commercial ZnO showed weaker and less uniform mineralization compared to green-synthesized ZnO, with fewer mineralized nodules even at Day 7. Green ZnO promoted superior mineralization and upregulated osteogenic markers, likely due to phytochemical capping, improved stability, and controlled Zn^{2+} release, which supports osteoblast activity and reduces oxidative stress. In contrast, commercial ZnO may impair mineralization due to excessive ROS and unregulated ion release.

3.12 Antibacterial and Antibiofilm Activity

Green-synthesized ZnO NPs showed superior antibacterial and antibiofilm efficacy against S. mutans and S. aureus compared to commercial ZnO, likely due to benefits conferred by phytochemical-mediated synthesis. (Table 4).

Disk diffusion results showed both ZnO nanoparticle types had strong antibacterial activity against S. mutans (inhibition zones ≈20–22 mm). Green ZnO NPs were more effective against S. aureus, with a larger inhibition zone (20 mm vs. 17 mm for commercial ZnO at 50 µg/mL) (Fig.16). Visual evidence confirmed the superior antibacterial effect of green ZnO NPs. (Table 5).

Green ZnO NPs demonstrated superior antibiofilm activity against S. aureus (~90% inhibition at 10 µg/mL) compared to commercial ZnO NPs (58.43% at the same dose). This highlights the enhanced biofilm penetration and disruption capabilities of the green-synthesized nanoparticles. (Table 6).

While both types of nanoparticles strongly inhibit S. mutans biofilms, comprehensive testing (MIC, inhibition zones, and antibiofilm assays) proves that green-synthesized ZnO NPs deliver superior and more consistent antimicrobial performance, particularly at lower concentrations. This highlights their strong potential for clinical and dental applications to control bacterial growth.

4. DISCUSSION

Developing multifunctional bone scaffolds that simultaneously promote osteogenesis and prevent bacterial infection remains a critical challenge. This study demonstrates that green-synthesized ZnO nanoparticles (NPs) via Anethum graveolens extract overcome the inherent limitations of commercial ZnO, establishing a highly effective, multifunctional coating for cortical bone scaffolds (12-14).

The distinct biological advantages of green ZnO NPs originate from their phytochemical functionalization. FTIR analysis confirmed that plant-derived compounds successfully capped the nanoparticles. This biological capping prevented severe agglomeration, yielding a uniform, mesoporous, cauliflower-like structure that deposited homogeneously onto the bone plates. In contrast, commercial ZnO formed compact, heterogeneous, and discontinuous clusters (15,16).

Crucially, this phytochemical surface modification resolved the dose-dependent cytotoxicity typically associated with ZnO. Commercial ZnO often induces cell death via rapid, unregulated Zn^{2+} burst release and excessive reactive oxygen species (ROS) generation. In contrast, the biological capping on green ZnO likely moderates ion release, mitigating oxidative stress and yielding a more than 12-fold increase in cytocompatibility (IC_{50} ≈ 321 µg/mL vs. 26 µg/mL) (17).

By maintaining cellular viability, green ZnO allowed MG-63 cells to harness the well-documented stimulatory effects of zinc on osteoblast activity (18). This controlled microenvironment resulted in the sustained upregulation of early (ALP), intermediate (COL1), and late-stage (OCN) osteogenic markers. Furthermore, Alizarin Red S staining confirmed that green ZnO drove robust, terminal extracellular matrix mineralization, whereas commercial ZnO impaired long-term maturation (19,20).

Finally, the functionalized scaffolds effectively addressed the risk of postoperative infection. While both nanoparticle types exhibited baseline antibacterial properties, green ZnO demonstrated superior bacteriostatic and antibiofilm efficacy, achieving nearly 90% biofilm inhibition against S. aureus at low concentrations (10 µg/mL) (21-23). This enhanced performance is attributed to the synergistic action of ZnO-mediated membrane disruption and the retained bioactive phytochemicals from the A. graveolens extract (24,25).

In summary, plant-mediated synthesis transforms ZnO from a potentially cytotoxic material into a highly biocompatible, osteoinductive, and infection-resistant biomaterial (26-30). Future in vivo studies utilizing critical-sized defect models are warranted to validate the long-term regenerative capacity of these green ZnO-coated scaffolds.

5. CONCLUSIONS

This study demonstrated the successful green synthesis of zinc oxide nanoparticles using Anethum graveolens extract and their effective incorporation into cortical bone plates to develop a multifunctional biomaterial for bone regeneration. The green-synthesized ZnO nanoparticles exhibited favorable physicochemical characteristics, improved coating homogeneity, and enhanced colloidal stability compared with commercial ZnO nanoparticles. Biological evaluation revealed strong antibacterial and antibiofilm activity, high cytocompatibility, and significantly enhanced osteogenic differentiation of MG-63 cells, evidenced by upregulation of ALP, COL1, and OCN together with increased matrix mineralization (The green-synthesized ZnO exhibited 12-fold higher IC_{50}, superior osteoinductive activity). Overall, these findings indicate that plant-mediated ZnO nanoparticles represent a promising bioactive nanomaterial for bone tissue engineering and infection-resistant regenerative biomaterials.

Conflict of Interest

The authors declare no conflict of interest.

Ethical Approval

No human participants or animals were involved in this study.

Patient Consent

Not applicable.

Funding

This research received no external funding.

Availability of Data

Available upon reasonable request.

Author Contributions

Luay Ahmed Hussein: designed the study work, performed the experiments, analyzed the data, wrote the manuscript. Othman Abubakir Omar; drafted and edited the manuscript, Azeez Abdullah Barzinjy supervising the green synthesis of the zinc oxide nanaoparticles.

REFERENCES

1. Giannoudis, P.V., Dinopoulos, H., Tsiridis, E. Bone substitutes: an update. Injury, 2005; 36:S20-S27. DOI: https://doi.org/10.1016/j.injury.2005.07.029

2. Oryan, A., Alidadi, S., Moshiri, A., Maffulli, N. Bone regenerative medicine. J Orthop Surg Res, 2014; 9:18. DOI: https://doi.org/10.1186/1749-799X-9-18
3. Rai, M., Yadav, A., Gade, A. Nanotechnology in biomedical applications. Biotechnol Adv, 2009; 27:76-83. DOI: https://doi.org/10.1016/j.biotechadv.2008.09.002
4. Zhang, G., Yang, J., Wang, J., Fang, Y., Shang, P. Nanoparticles in bone tissue engineering. Nanoscale Adv, 2024; 6:1957-1973. DOI: https://doi.org/10.1039/D3NA00851G
5. Prasad, A.S. Discovery of human zinc deficiency. Nutrition, 2013; 29:124-129.
6. Yamaguchi, M. Role of zinc in bone formation. Mol Cell Biochem, 2010; 338:241-254. DOI: https://doi.org/10.1007/s11010-009-0358-0
7. Xie, Y., He, Y., Jin, T., Shi, X. Antibacterial activity of ZnO nanoparticles. Mater Sci Eng C, 2017; 78:507-515.
8. Iravani S. Green synthesis of metal nanoparticles using plants. Green Chem, 2011; 13:2638-2650. DOI: https://doi.org/10.1039/c1gc15386b
9. Singh, J., Dutta, T., Kim, K.H., Rawat, M., Samddar, P., Kumar, P. Green synthesis of nanoparticles. J Nanobiotechnol, 2018; 16:84. DOI: https://doi.org/10.1186/s12951-018-0408-4
10. Bose, S., Roy, M., Bandyopadhyay, A. Bone tissue engineering scaffolds. Trends Biotechnol, 2012; 30:546-554. DOI: https://doi.org/10.1016/j.tibtech.2012.07.005
11. Tang, W., Pan, P., Chen, T., Wang, J., Cui, X., Liu, W. ZnO nanoparticle-reinforced scaffolds for bone regeneration. Colloids Surf B Biointerfaces, 2025; 245:114199. DOI: https://doi.org/10.1016/j.colsurfb.2024.114199
12. Zhang, Y., Li, X., Zhao, H. Zinc-based nanomaterials for bone regeneration and tissue engineering. Bioact Mater, 2024; 29:456-470.
13. Shnawa, B.H., Jalil, P.J., Mhammedsharif, R.M., Faqe, B.A., Ahmed, M.H., Ibrahim, H.N., et al. Synthesis, characterization, and evaluation of antioxidant, anti-inflammatory, and antimicrobial activities of zinc oxide nanoparticles using adiantum Capillus-veneris L. leaf extract. Part Part Syst Charact, 2024; 41:2400005. DOI: https://doi.org/10.1002/ppsc.202400005
14. Jalil, P.J., Mhamedsharif, R.M., Shnawa, B.H., Hamad, S.M., Aspoukeh, P., Wsu, K.W., et al. Biosynthesis of ZnO nanoparticles using washingtonia filifera seed extract and assessment of their anti-inflammatory and antimicrobial efficacy. J Clust Sci, 2024; 36:31. DOI: https://doi.org/10.1007/s10876-024-02761-3
15. Chehhat, K., Chehhat, A.E., Kara, R., Yacoub, A., Salhi, F., Mecif, A., et al. Study of effect of high annealing temperature on the photocatalytic activity of ZnO thin films prepared by dip-coating method. Transit Met Chem, 2025; 50:335-343. DOI: https://doi.org/10.1007/s11243-024-00627-1
16. Ahmed, M.H., Jalil, P.J., Shnawa, B.H. Green synthesis of ZnO nanoparticles using plant extracts for biomedical applications. rt. Part Syst Char, 2024; 41:2400005.
17. Chehhat, K., Chehhat, A.E., Kara, R., et al. Photocatalytic and structural properties of ZnO nanostructures. Transit Met Chem, 2025; 50:335-343. DOI: https://doi.org/10.1007/s11243-024-00627-1
18. Jahan Tamanna, N., Sahadat Hossain, M., Mohammed Bahadur, N., Ahmed, S. Green synthesis of Ag2O & facile synthesis of ZnO and characterization using FTIR, bandgap energy & XRD (Scherrer equation, Williamson-Hall, size-train plot, Monshi- Scherrer model). Results Chem, 2024; 7:101313. DOI: https://doi.org/10.1016/j.rechem.2024.101313
19. Sirelkhatim, A., Mahmud, S., Seeni, A., Kaus, N.H.M., Ann, L.C., Bakhori, S.K.M., et al. Zinc oxide nanoparticles: antibacterial activity and mechanisms. Nano-Micro Lett, 2015; 7:219-242. DOI: https://doi.org/10.1007/s40820-015-0040-x
20. Hernández-Sierra, J.F., Ruiz, F., Pena, D.C., Martínez-Gutiérrez, F., Martínez, A.M., e Jesús Pozos Guillén, A., et al. Antimicrobial sensitivity of Streptococcus mutans to nanoparticles. Nanomedicine, 2008; 4:237-240. DOI: https://doi.org/10.1016/j.nano.2008.04.005
21. Hosseinzadeh, E., Foroumadi, A., Firoozpour, L. Phytochemical capping agents in green synthesis of metal oxide nanoparticles. Inorg Chem Commun, 2022; 146:110183.
22. Alshehri AA, et al. Green synthesis of zinc oxide nanoparticles for biomedical applications. Int J Nanomedicine, 2025; 20:4127-4152.
23. Alshahrani, M.M., et al. Osteogenic differentiation potential of green synthesized ZnO nanoparticles in MG-63 cells. Mater Sci Eng C, 2021; 120:111676.
24. Yamaguchi, M., et al. Zinc regulation of Runx2 expression via BMP-2 signaling in osteoblasts. J Nutr Health Food Eng, 2018; 8:23-29.
25. Liu, X., et al. ZnO nanoparticle-based biomaterials promoting osteogenesis and angiogenesis. Front Med, 2025; 12:1729401.
26. Wang, Y., Li, J., Zhao, H. Antibacterial mechanisms of nano-zinc oxide materials. Mater Chem Phys, 2023; 295:127095.
27. Raghupathi, K.R., Koodali, R.T., Manna, A.C. Size-dependent bacterial growth inhibition and mechanism of antibacterial activity of zinc oxide nanoparticles. Langmuir, 2011; 27(7):4020-4028. DOI: https://doi.org/10.1021/la104825u
28. Salem, W., Leitner, D.R., Zingl, F.G., Schratter, G., Prassl, R., Goessler, W., et al. Antibacterial activity of silver and zinc nanoparticles. Int J Med Microbiol, 2015; 305(1):85-95. DOI: https://doi.org/10.1016/j.ijmm.2014.11.005
29. Kalishwaralal, K., Deepak, V., Pandian, S.R.K., et al. Biofilm inhibition by nanoparticles. Colloids Surf B Biointerfaces, 2010; 79(2):340-344. DOI: https://doi.org/10.1016/j.colsurfb.2010.04.014
30. Shubha, P., Gowri, S. Phytochemical capping mediated ZnO nanoparticles. Mater Sci Eng C, 2018; 93:381-90.

TABLES

Table 1. The primer sequences

	Forward Primer	Reverse Primer	Length (bp)
ALP	5′-CAACGAGGTCATCTCCGTGATG-3′	5′-TACCAGTTGCGGTTCACCGTGT-3′	129
COL1	5′-GATTCCCTGGACCTAAAGGTGC-3′	5′-AGCCTCTCCATCTTTGCCAGCA-3′	107
OCN	5′-CGCTACCTGTATCAATGGCTGG-3′	5′-CTCCTGAAAGCCGATGTGGTCA-3′	123
GAPDH	5′-GTCTCCTCTGACTTCAACAGCG-3′	5′-ACCACCCTGTTGCTGTAGCCAA-3′	131

Table 2. Crystallite size of ZnO for bone plate coated with commercial ZnO NPs

2θ (degree)	FWHM (°)	D (nm)	Average D (nm)
31.1807	0.9446	9.119529	10.10
35.7546	0.7872	11.075106	

Table 3. Crystallite size of ZnO for bone plate coated with green-synthesized ZnO NPs

2θ (degree)	FWHM (°)	D (nm)	Average D (nm)
31.0218	0.4723	18.232022	16.17
33.7225	0.4723	18.357180	
35.6355	0.4723	18.453115	
46.6818	0.9446	9.566923	
55.9154	0.5510	17.048396	
62.1359	0.6298	15.380910	

Table 4. Minimum Inhibitory Concentration (µg/mL) value of both commercial and green zinc oxide nanoparticles

ZnO nanoparticles	Streptococcus mutans		Staphylococcus aureus	
	Concentrations (µg/mL)	Optical density (600nm)	Concentrations (µg/mL)	Optical density (600nm)
Commercial	10	0.104	50	0.19
Green	10	0.091	50	0.047

Table 5. The diameter of inhibition zones (mm) of green and commercial zinc oxide nanoparticles at different concentrations against bacterial isolates

Bacterial isolates	Zinc oxide nanoparticles (IZD mm)									
	Green NPs					Commercial NPs				
	10	25	50	75	100	10	25	50	75	100
Streptococcus mutans	22	22	22	20	21	22	22	22	22	21
Staphylococcus aureus	15	16	20	15	18	15	15	17	15	15

Table 6. DPPH scavenging (%) for commercial and green synthesized zinc oxide nanoparticles

Bacterial isolates	Zinc Oxide nanoparticles									
	Green NPs					Commercial NPs				
	10	25	50	75	100	10	25	50	75	100
Streptococcus mutans	88.96	89.56	92.97	93.37	93.78	87.55	87.95	87.95	89.76	91.16
Staphylococcus aureus	90.56	90.96	90.96	90.96	91.16	58.43	64.26	68.67	77.31	86.35

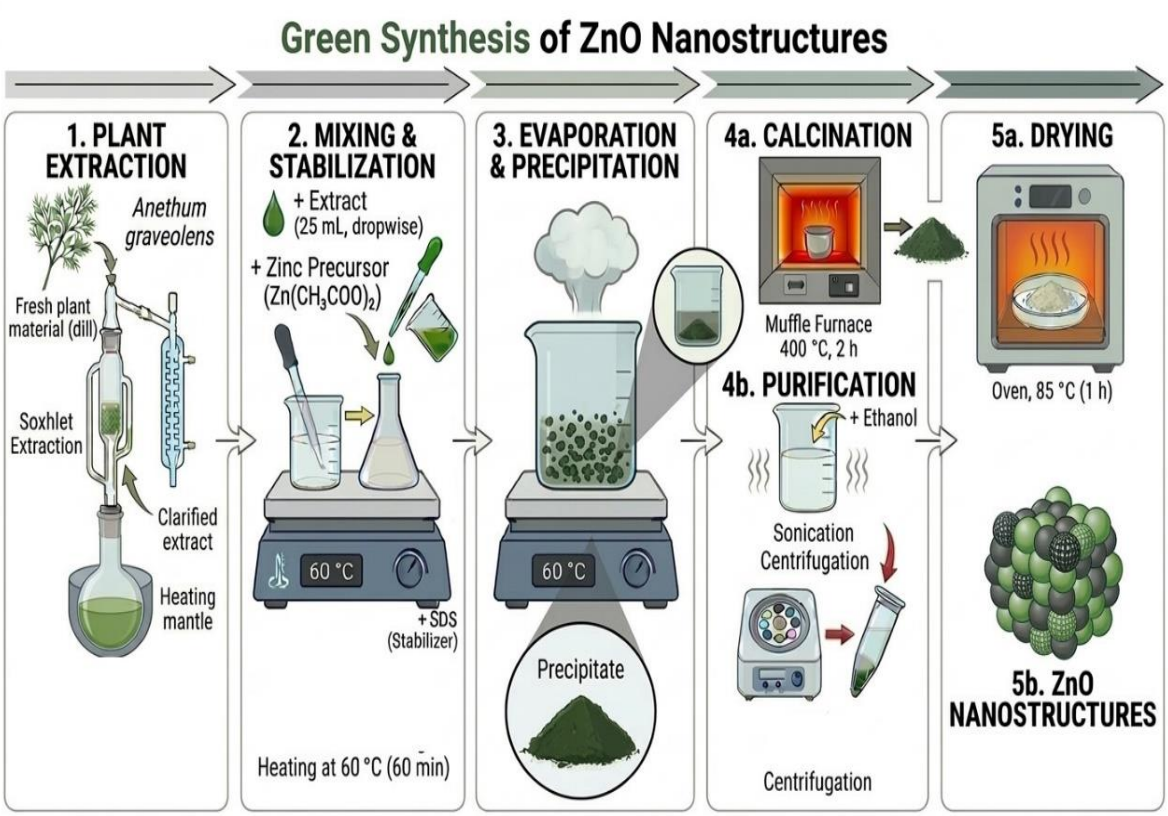

Scheme 1: Green synthesis of ZnO nanostructures using Anethum graveolens extract.

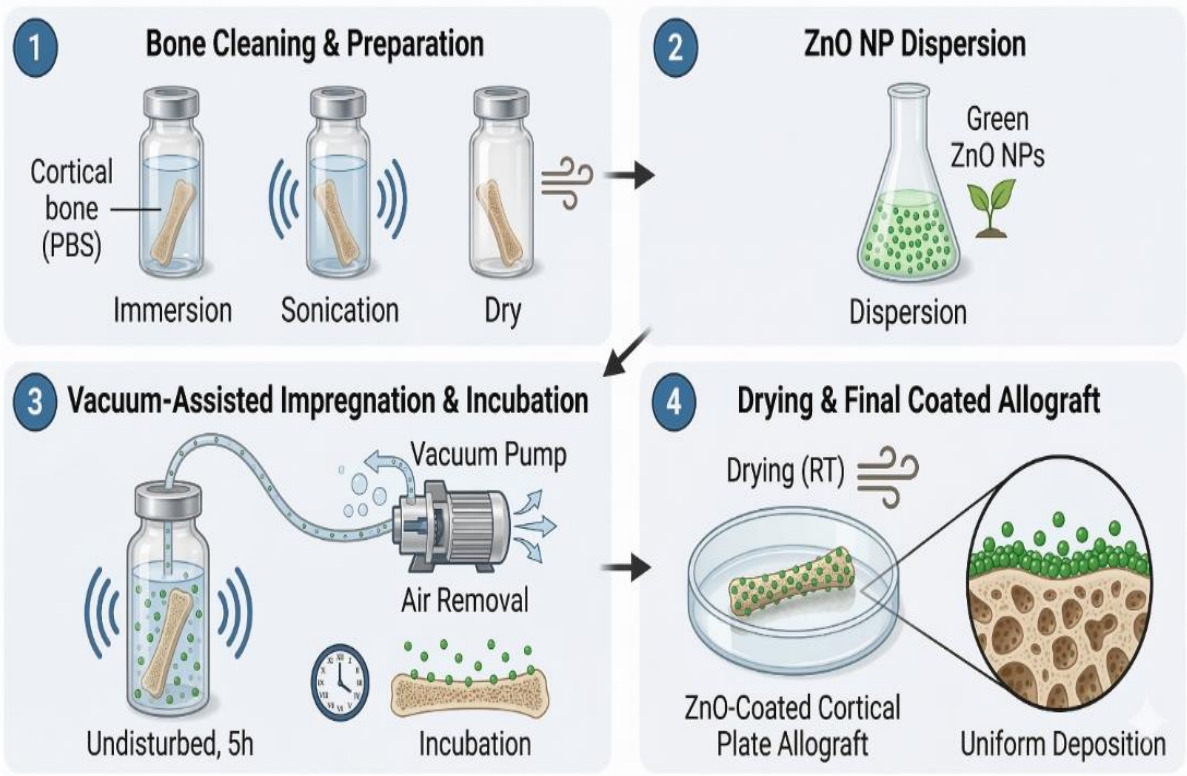

Scheme 2: Schematic illustration of the surface coating process for a cortical plate allograft using green-synthesized ZnO nanoparticles.

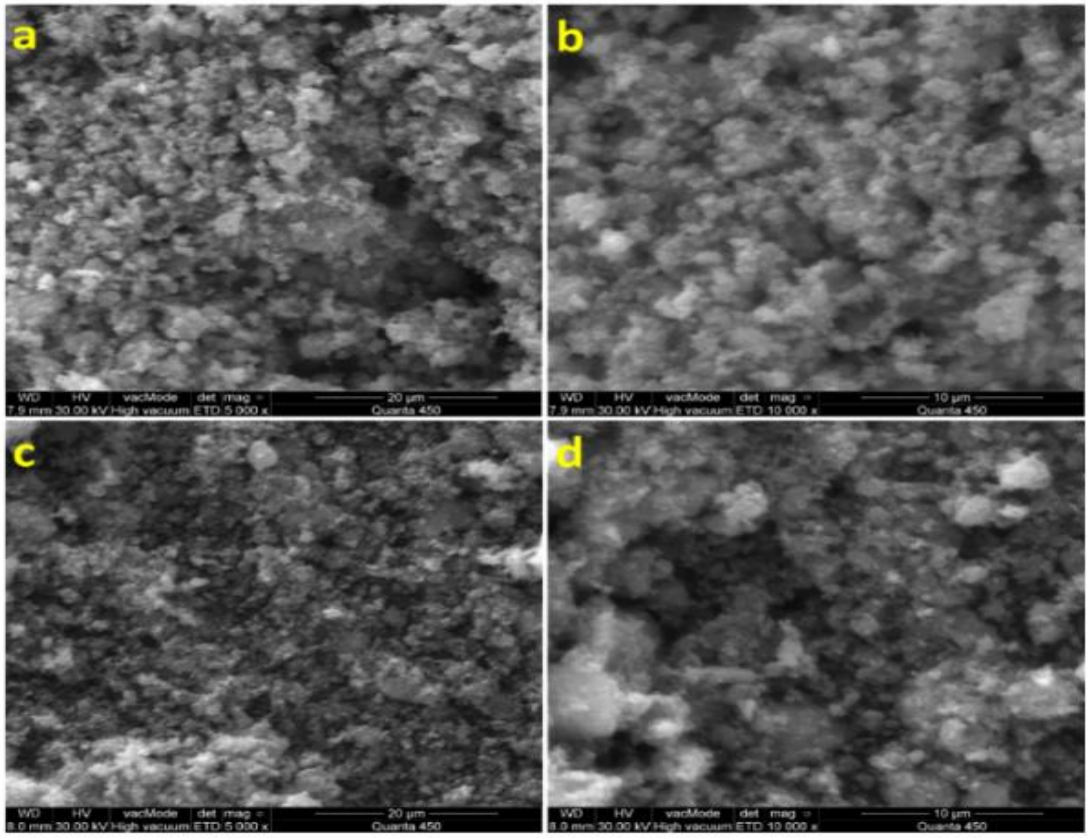

Fig.1. SEM micrographs of ZnO samples: (a, b) green-synthesized ZnO nanoparticles and (c, d) commercial ZnO nanoparticles at different magnifications.

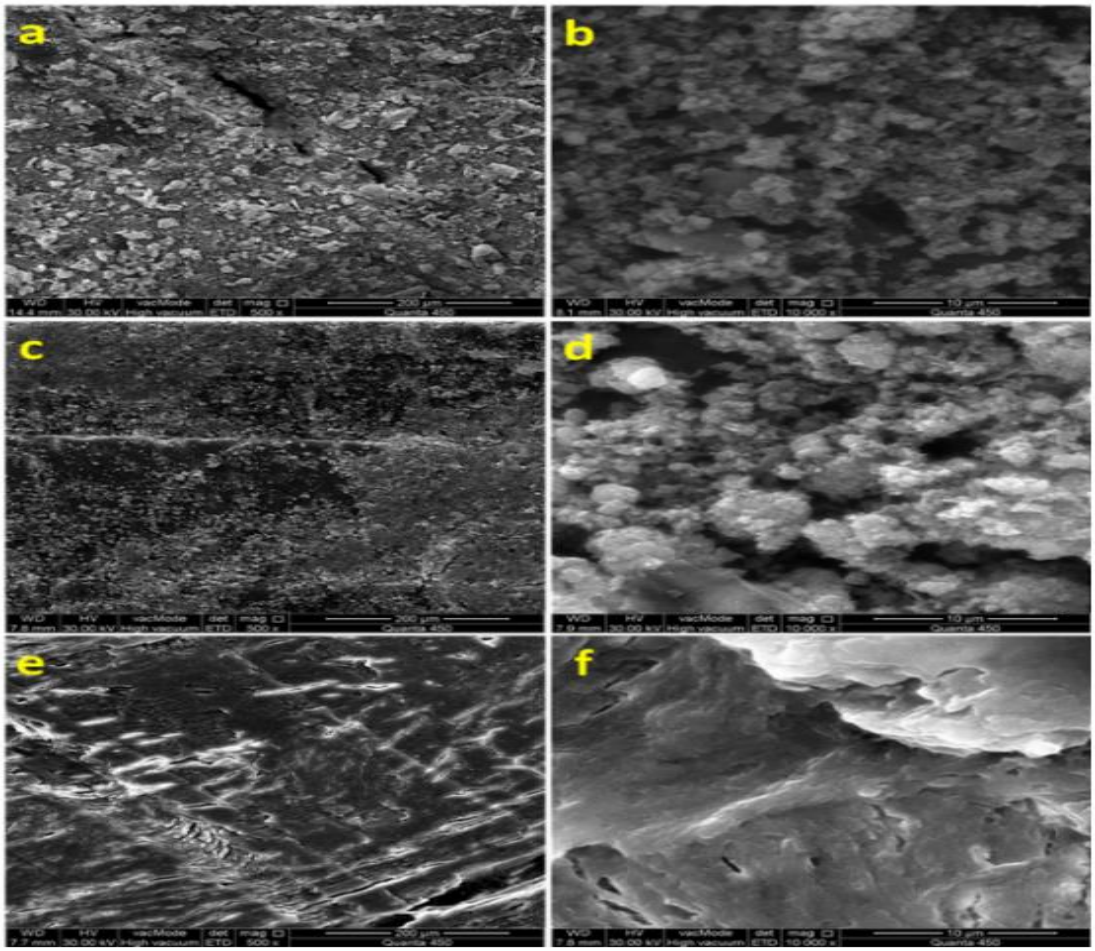

Fig.2. SEM of cortical bone plates coated with ZnO nanoparticles: (a, b) bone plate coated with green-synthesized ZnO and (c, d) bone plate coated with commercial ZnO and (e,f) uncoated cortical bone plate.

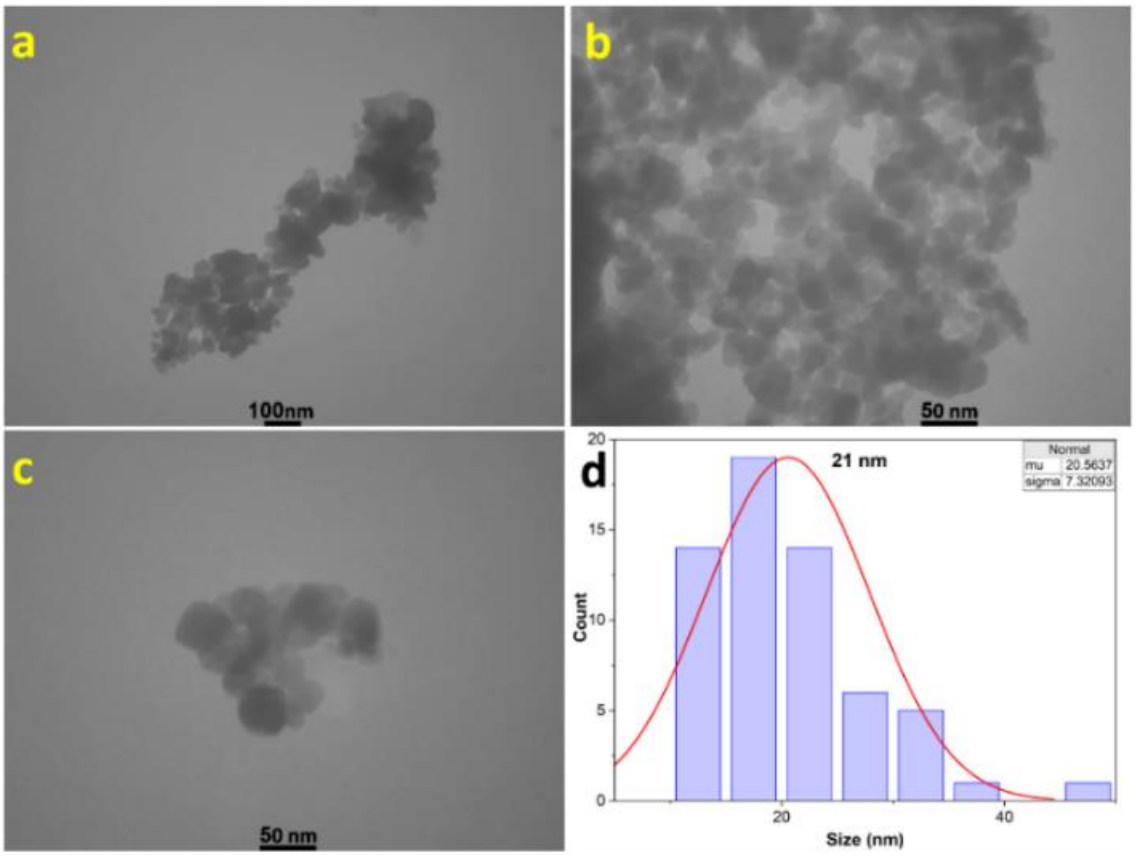

Fig.3. TEM images of green-synthesized ZnO nanoparticles and (d) particle size distribution histogram.

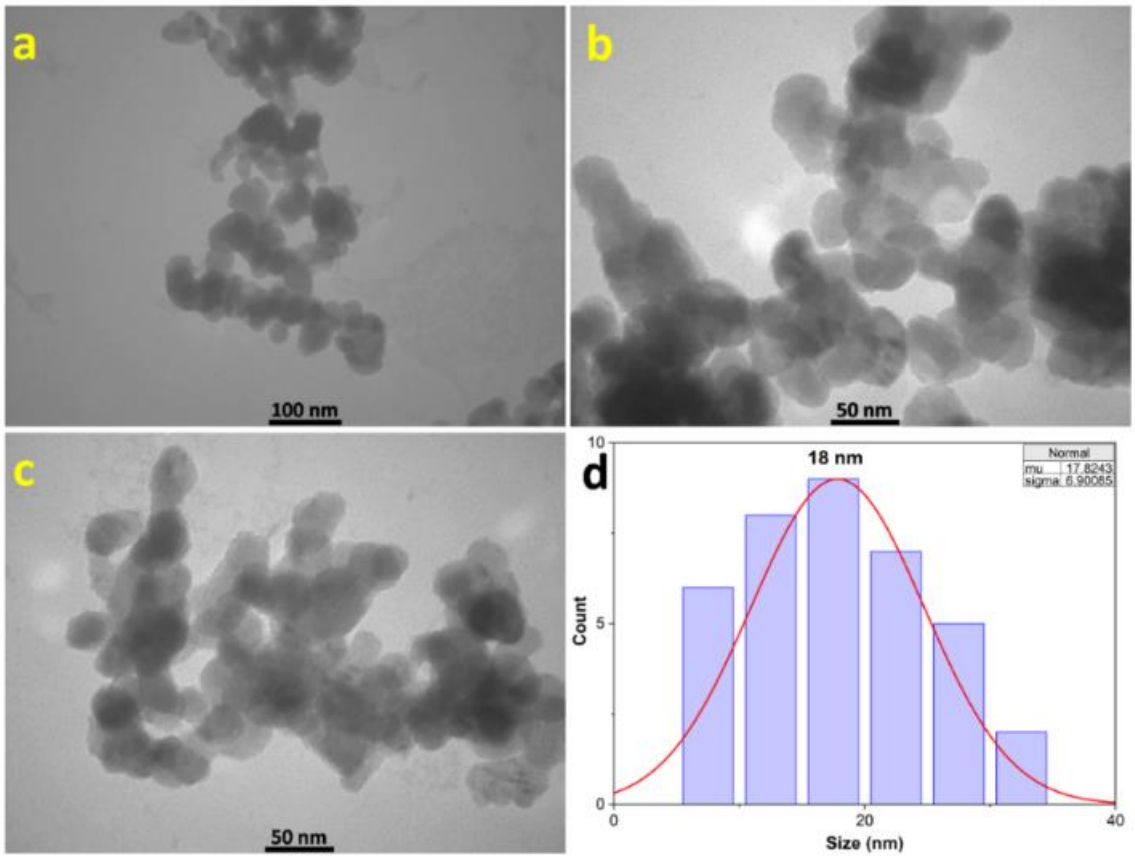

Fig .4. TEM images of commercial ZnO nanoparticles and (d) particle size distribution histogram.

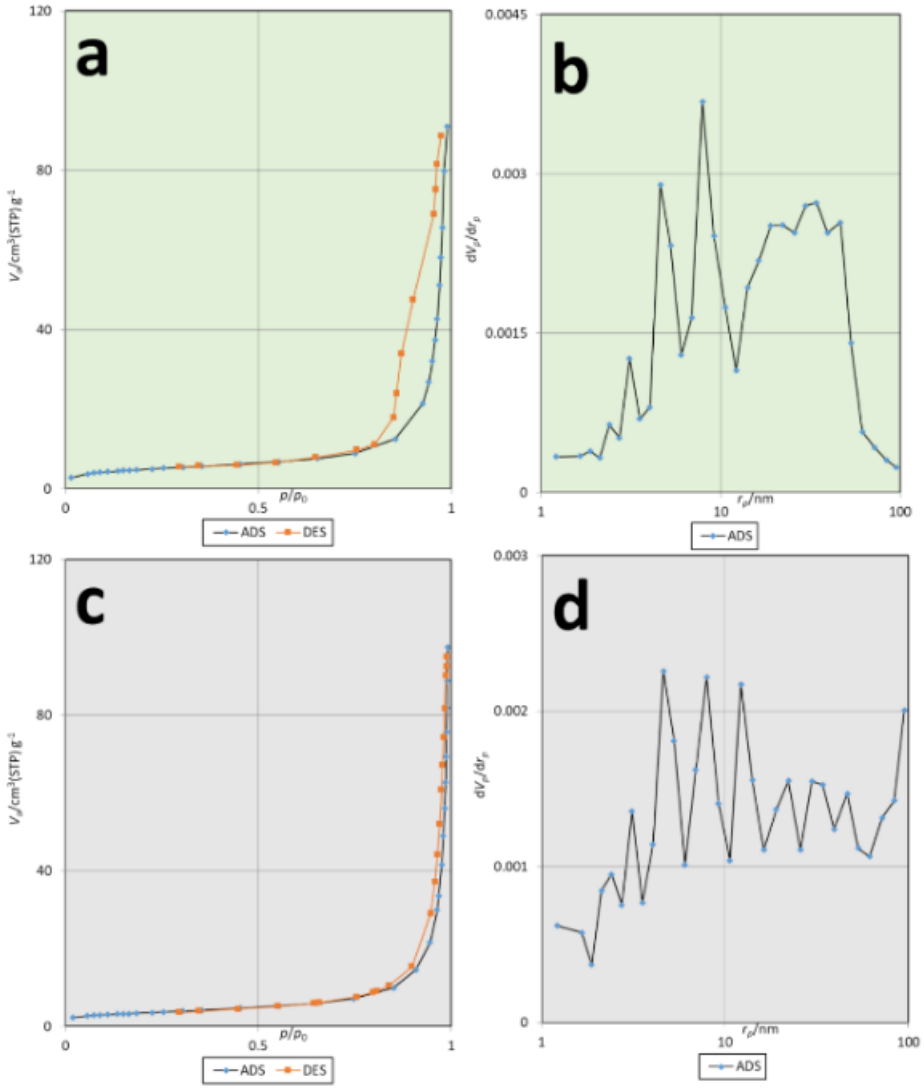

Fig.5. Nitrogen adsorption–desorption and BJH pore-size distribution of ZnO samples: (a, b) commercial ZnO nanoparticles and (c, d) green-synthesized ZnO nanoparticles.

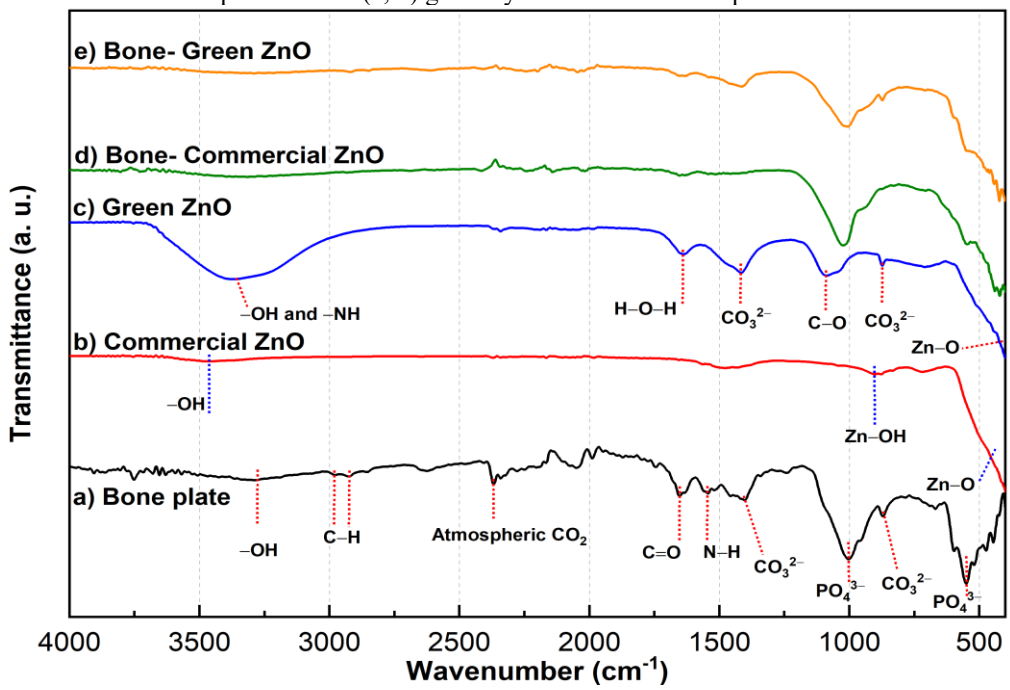

Fig.6. Stacked FTIR spectra of (a) uncoated cortical bone plate, (b) commercial ZnO nanoparticles, (c) green ZnO nanoparticles, (d) bone plate coated with commercial ZnO, and (e) bone plate coated with green-synthesized ZnO.

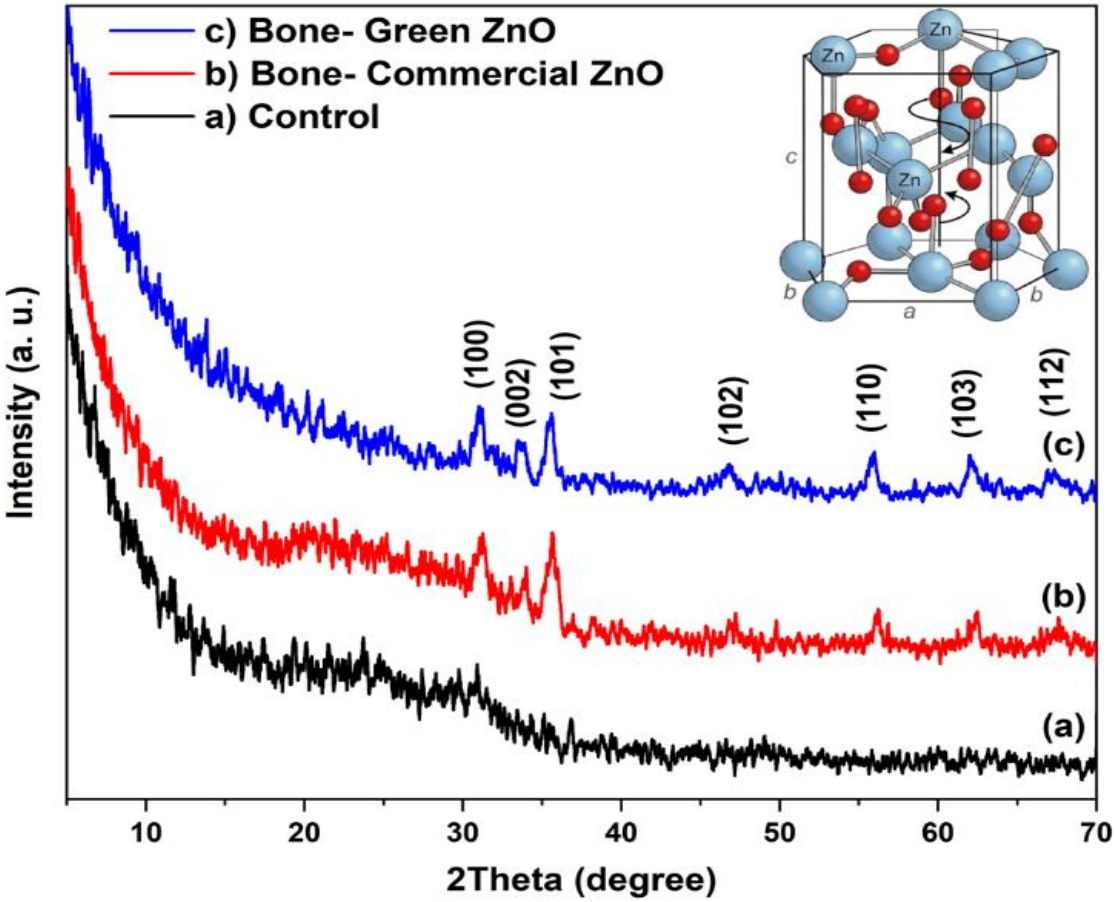

Fig.7. X-ray diffraction (XRD) patterns of (a) uncoated cortical bone plate (control), (b) bone plate coated with commercial ZnO nanoparticles, and (c) bone plate coated with green-synthesized ZnO nanoparticles.

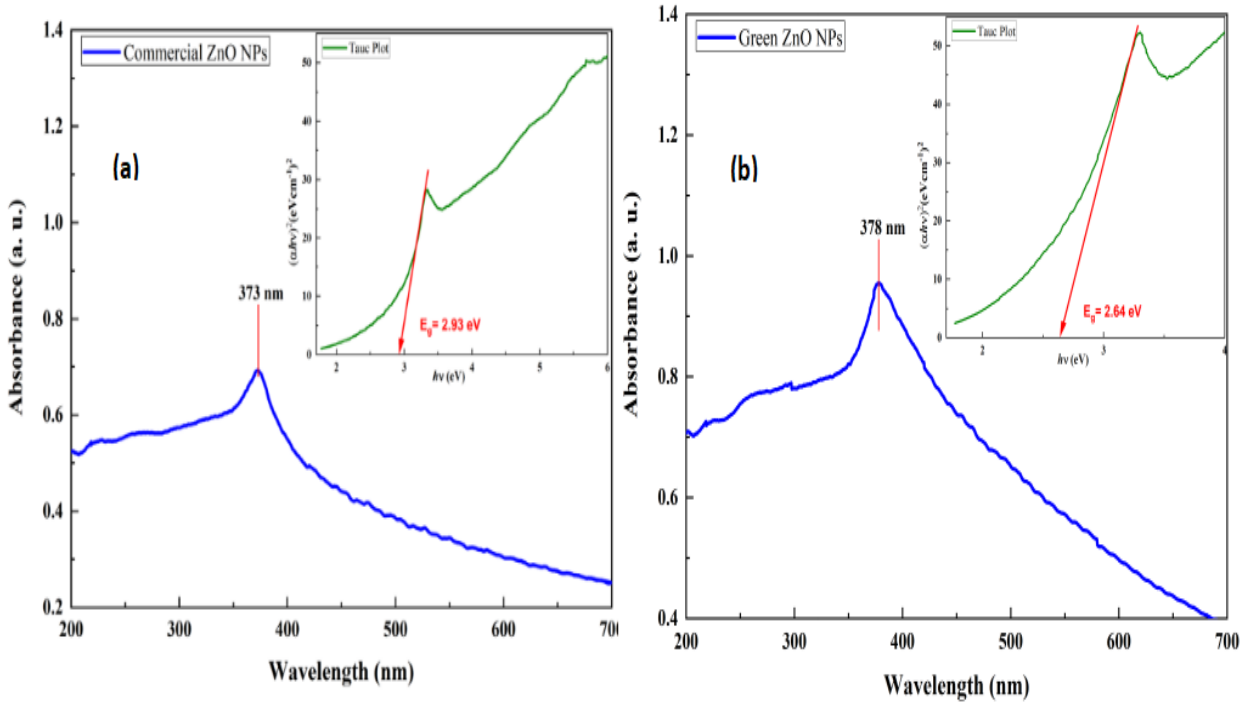

Fig.8. UV–Vis absorption spectra and corresponding Tauc plots of (a) commercial ZnO nanoparticles and (b) green-synthesized ZnO nanoparticles.

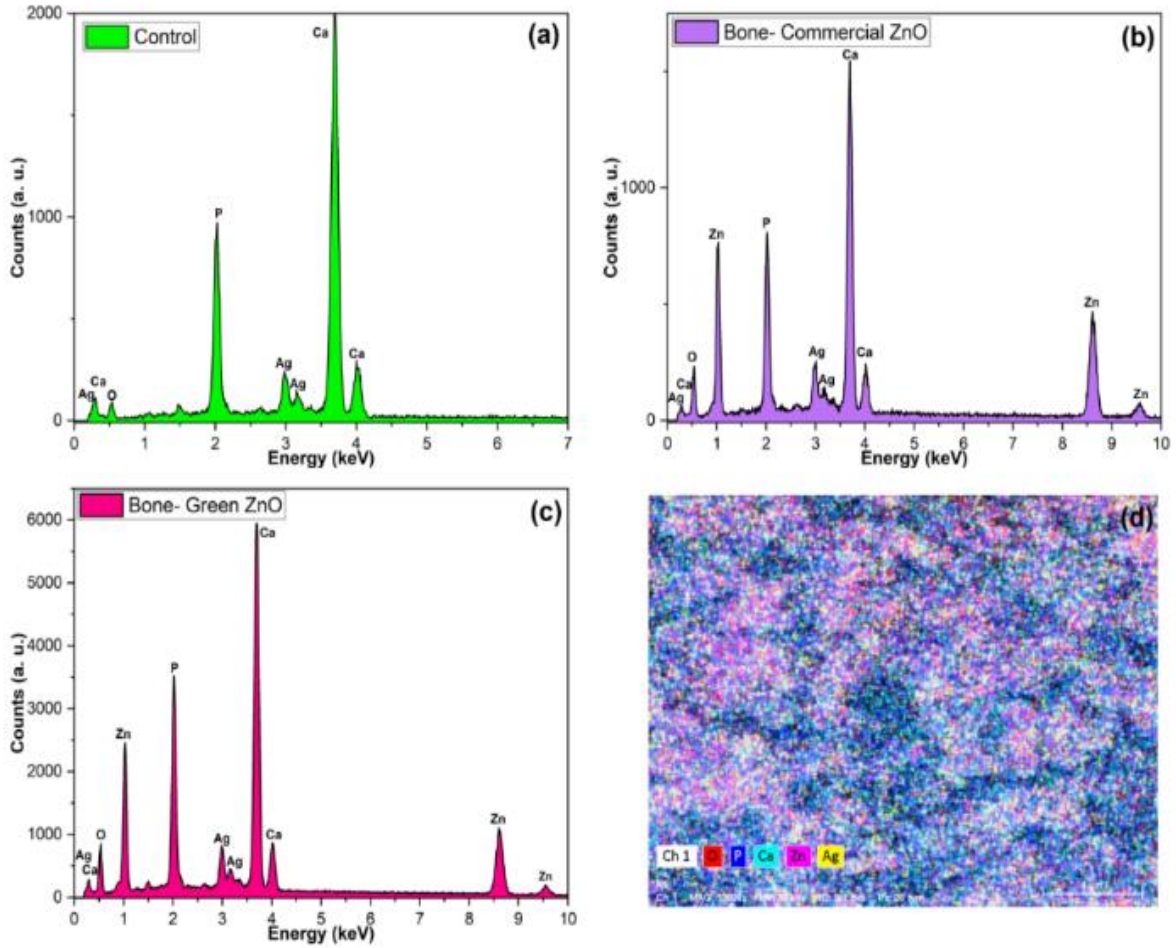

Fig.9. EDX spectra of (a) uncoated cortical bone plate, (b) bone plate coated with commercial ZnO nanoparticles, and (c) cortical bone plate coated with green-synthesized ZnO nanoparticles; (d) elemental mapping of the green-ZnO-coated bone plate.

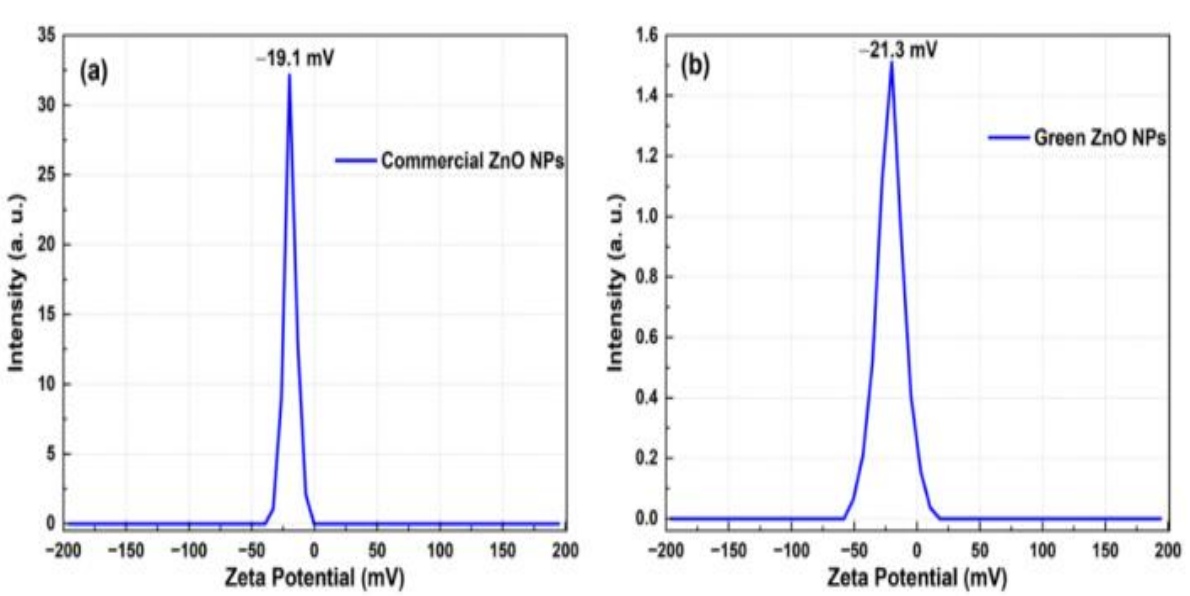

Fig.10. Zeta-potential distributions of (a) commercial ZnO nanoparticles and (b) green-synthesized ZnO nanoparticles.

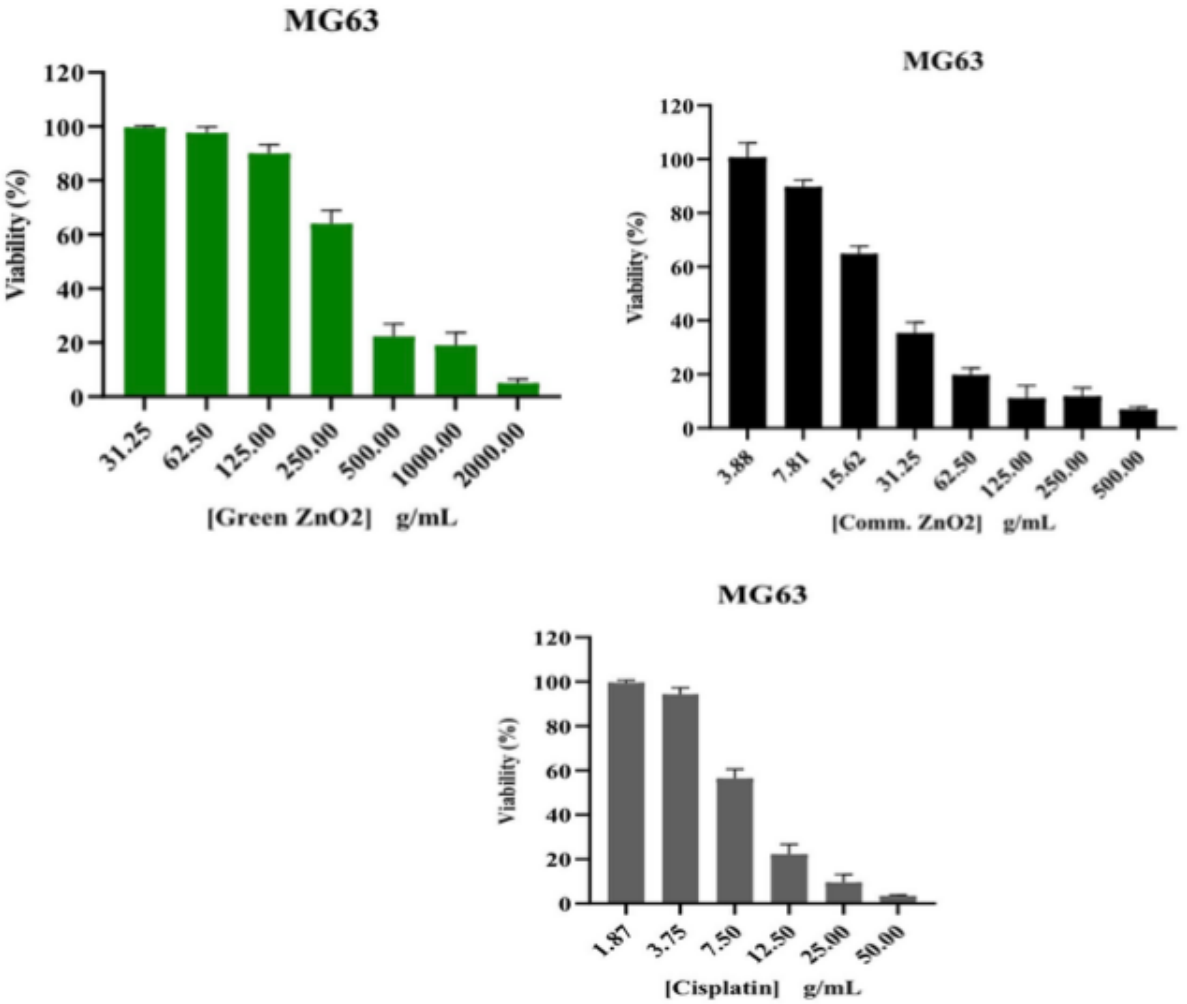

Fig 11. Cytocompatibility evaluation of green synthesized ZnO nanoparticles, commercial ZnO nanoparticles, and Cisplatin using the MG-63

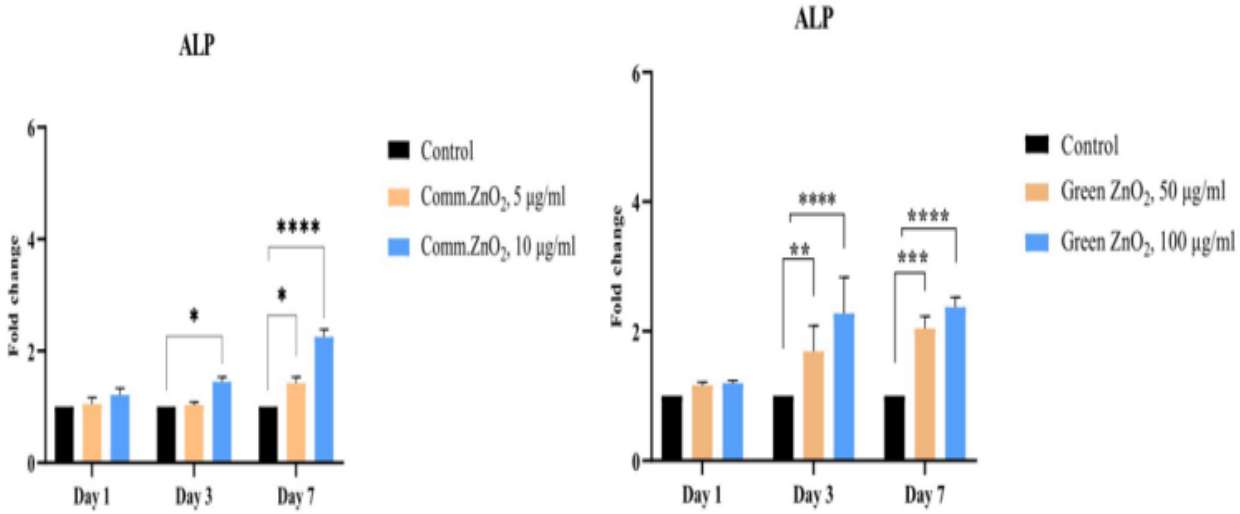

Fig12. ALP expression in commercial and green ZnO NP.

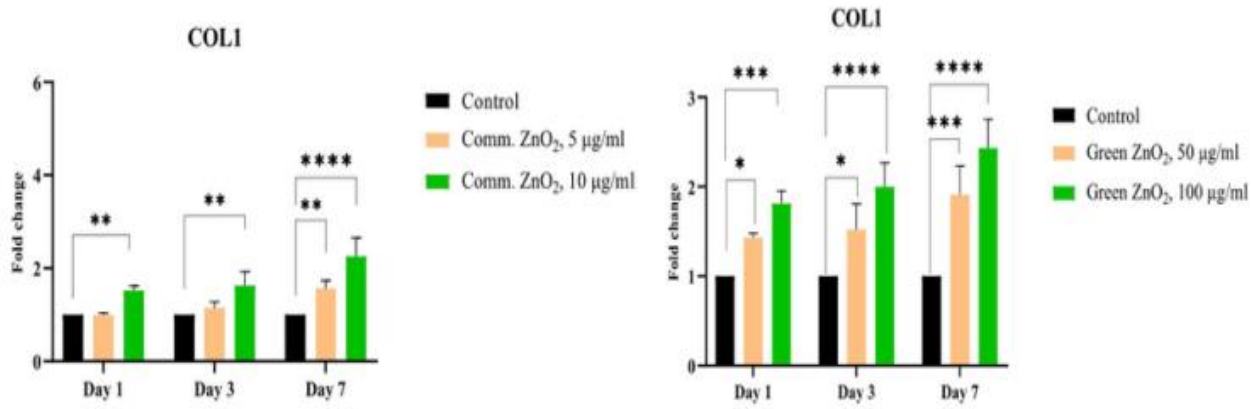

Fig 13. COL1 expression in commercial and green ZnO NP.

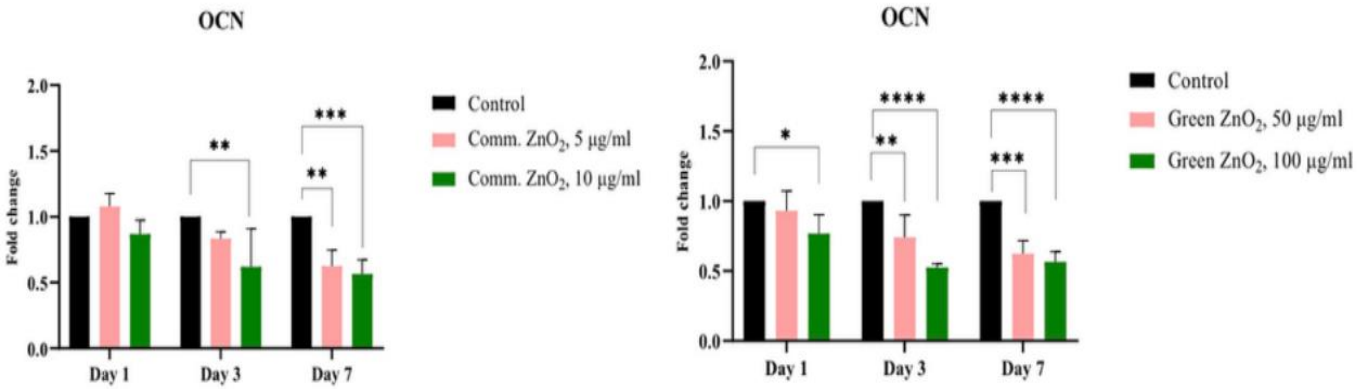

Fig 14. OCN expression in commercial and green ZnO NP.

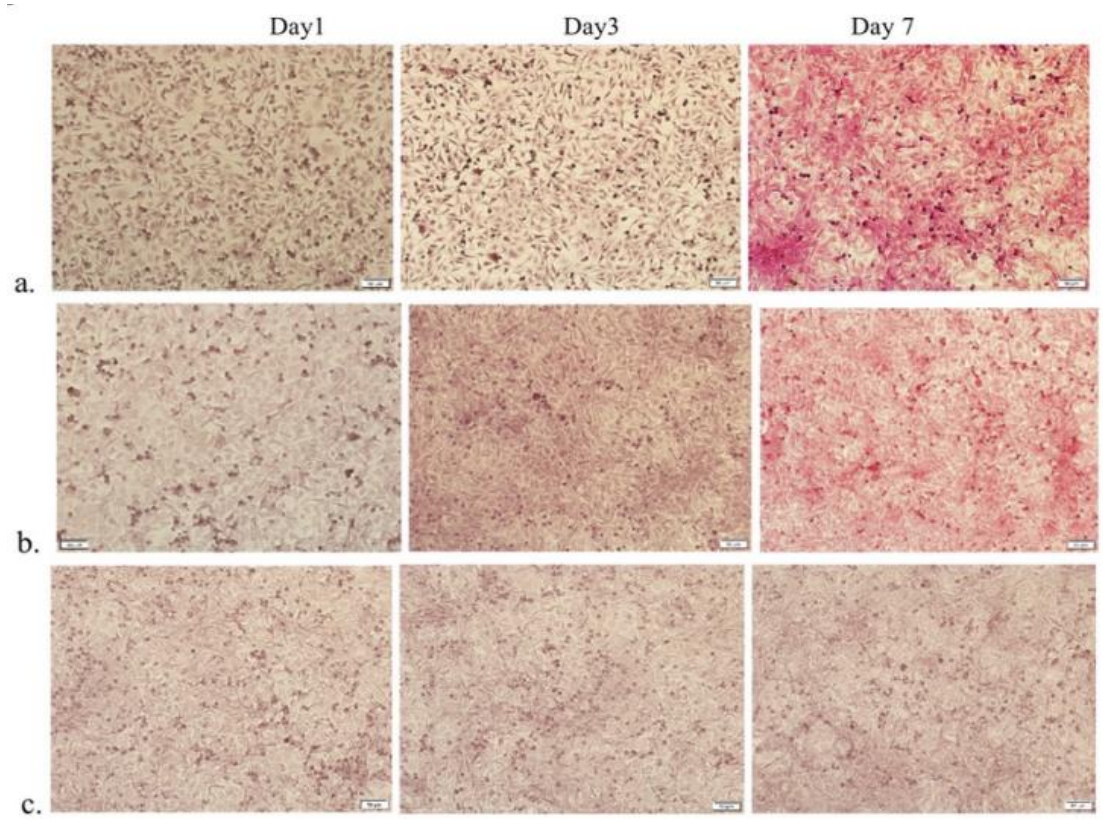

Fig 15. Extracellular matrix mineralization in MG-63 cells a. green synthesis ZnO_NP, b. commercial ZnO_ NP, c. control.

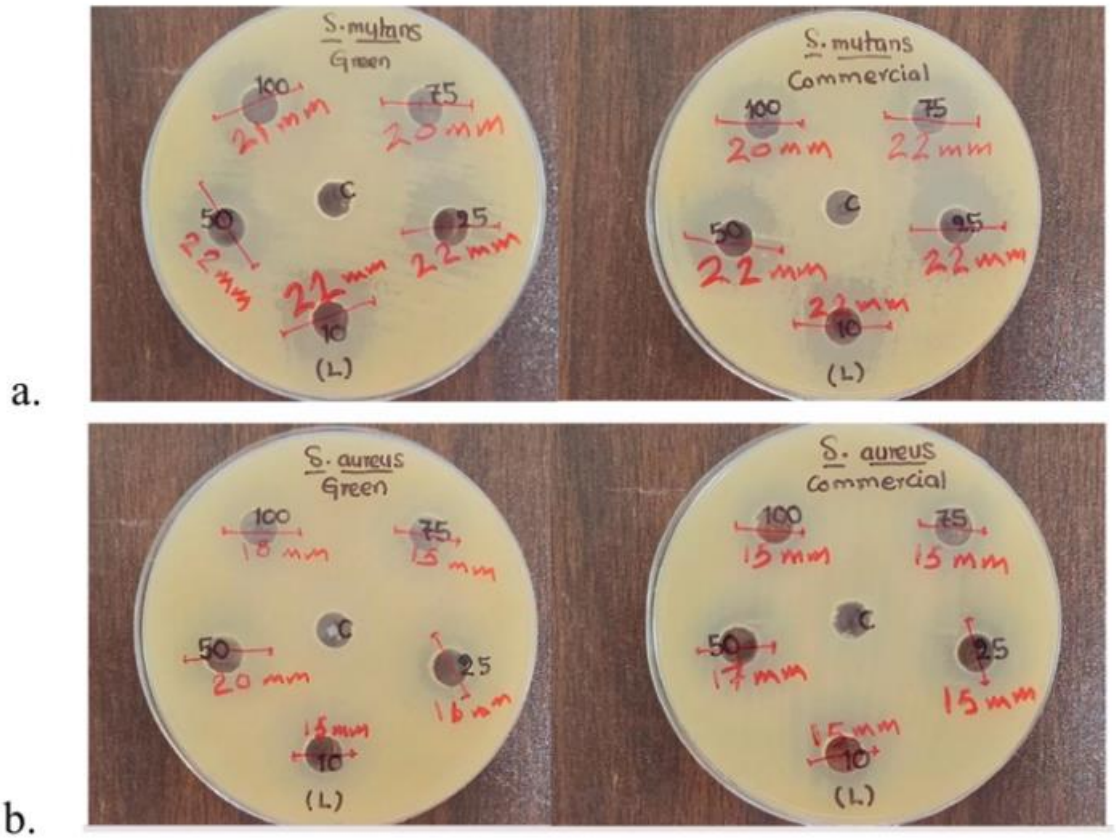

Fig 16. Formation of zone of inhibition against a. Streptococcus mutans b. Staphylococcus aureus using green ZnO NPs and commercial ZnONPs.